

ORIGINAL ARTICLE

Modeling and Optimization of Electrostatic Film Actuators Based on the Method of Moments

Wenguang Wang, Dongliang Fan, Renjie Zhu, Peisong Wang, Yonghua Zhao, and Hongqiang Wang

Abstract

Electrostatic film actuators represent a promising new approach to drive a soft robot, but they lack a comprehensive model to link the design parameters and actuation performance, making actuator design and parameter optimization challenging. To solve this problem, we build a mathematical model based on the method of moments by assuming that each electrode consists of a large number of line charges. This model can directly deduce fluctuation in thrust and adhesive forces during actuator movement, as well as the distribution of electric potential and field strength, for analysis and optimization. It consumes shorter computing time and fewer computing resources, but with comparable accuracy, in comparison with previous indirect means. It is validated by results from both previous studies and on-site experiments. Based on this model, we generate numerous values of actuator output force for different structural parameters. By analyzing the tendency, we summarize a parameter optimization workflow and write an open-sourced program as an example to facilitate the parameter selection for actuator design starting from scratch.

Keywords: electrostatic actuators, electrostatic film actuators, method of moments, optimization

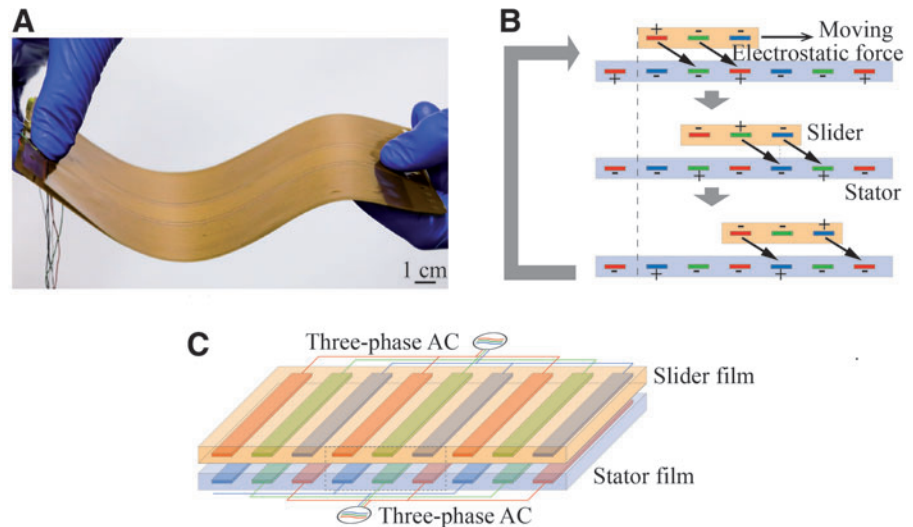
Objective

ELECTROSTATIC ACTUATORS ARE attracting increasing interest from researchers recently due to their outstanding metrics of being compliant, lightweight, and low cost.¹⁻⁷ Among them, electrostatic film actuators (EFAs) represent an emerging soft actuation technique in the last decades.^{8,9} A typical EFA comprises a stator film and a slider film made of identical structure of multiple phase electrodes, as shown in Figure 1A. Supplied with high voltage, unlike charges are induced in the electrodes of the films, which generate an attractive force, as shown in Figure 1B. When we simply shift the electrical polarity of electrodes in a specific order, the slider moves, by steps, laterally with respect to the stator. By repeating this switch order, the slider film slips continuously. To improve movement smoothness, generally, voltages are smooth curvatures such as sine waves, as shown in Figure 1C. An EFA has two distinct advantages compared with most of the soft actuators such as pneumatic actuation and electroactive polymers.¹⁰⁻¹² First, an EFA has better movement accuracy (several micrometers) and controllability based on the fine electrode and synchronous moving mechanism,¹³

similar to the conventional stepper motor, while other soft actuators are difficult to control due to nonlinear material properties such as hysteresis and creep.^{14,15} Second, an EFA could achieve a large elongation because the moving part of an EFA (i.e., the slider film) is independent of the stationary part (i.e., the stator film), while traditional soft actuators are usually as a whole unit and work on the mechanism of strain-induced deformation.^{16,17} Therefore, an EFA has great application potential in various scenarios, particularly those requiring large stroke and high-precision position control, as well as compliance, such as surgical robots, wearable robots, and inspection robots.¹⁸⁻²⁰

However, this novel research context still lacks a comprehensive mathematical model to link the fundamental parameters of actuators (e.g., geometrical and electrical specifications) and the output performance (mainly, e.g., force), although recent researches reveal important insights into this field. Previous researchers established a mathematical model of the EFA, but the capacitance matrix of the model needs to be measured through complex and time-consuming experiments.^{21,22} After that some other researchers started to find the capacitance matrix of electrodes

FIG. 1. The working mechanism of EFAs. (A) The flexibility of EFAs. (B) The steps of movement in a circle with a simple electrical polarity shift on the electrodes. (C) The configuration of an EFA. EFA, electrostatic film actuator. Color images are available online.



from the patterns' geometrical parameters using the finite element method (FEM) instead of experiments.^{23,24} Although these methods have become common in the modeling of EFA, they have the following disadvantages:

- (1) The previous methods are based on two steps: calculating the capacitance matrix from initial parameters and then calculating force from the capacitance matrix. In either step, the calculation involves fitness and simplification, with the sacrifice of accuracy.
- (2) The capacitance matrix was usually achieved by experiments or FEM previously. These methods are not adequate to support the design from scratch, and the latter consumes abundant computing resources and time.
- (3) These methods did not consider the normal attractive force between two films and therefore the influence of friction is not embedded in the calculation of thrust force.

Therefore, this work aims to establish a comprehensive model from the fundamental parameters, including dimensional parameters, material properties, and electrical settings, for the actual thrust force.

Substantially, the thrust force of an EFA is an electrostatic attractive or repulsive force of distributed charge on the electrode array. As a result, if the charge distribution on the electrode array at given voltages is obtained, we could calculate the thrust force of the actuator using Coulomb's law. There are three common methods to calculate charge distribution of a complex electrode geometry in the electrostatic field: FEM/FDM (finite difference method), conformal mapping (CM), and method of moments (MoM).^{25,26} FEM/FDM uses electric potential as an independent variable to solve differential equations and needs to mesh the three-dimensional space. It is applicable for complex geometry, and thus the computing accuracy is related to the number of elements. CM transforms irregular shapes into a regular shape and calculates the related variables under classical models of parallel-plate capacitance. This method is only suitable for some relatively simple situations to obtain exact values theoretically. MoM is an integral method that solves

Maxwell's equation in the integral form in contrast to FEM/FDM using differential equations. Therefore, MoM needs only to mesh electrodes and thus takes a shorter computation time and fewer computing resources and has comparable accuracy, compared with FEM.

In an EFA, the electrode pattern is a two-layer electrode array, and each electrode has a rectangular cross section. Since electrodes in the two layers are not exactly overlapped, sometimes its calculation is out of the capability of CM. FEM/FDM instead is capable of solving such a complex shape, but it has to mesh the large space with fine features with a large number of elements, which wastes huge amounts of computational resources. If using MoM, meshing the insulating space is not necessary anymore. Besides, we combine the long and thin features of every electrode in actuator films with traditional MoM, considering an electrode as multilines of charge placed side by side. MoM with the line charge as its fundamental element can greatly reduce the computation burden when using the electric potential formula of an infinitely long, uniformly distributed line charge. Thus, MoM based on line charges (MoM-Line) is the most suitable method in our study.

In this article, we build a comprehensive model of EFAs using MoM based on line charges and mathematically obtain the direct relationship between the initial parameters and actuator performance. Using this model, we analyze multiple initial parameters, including width a , space s , pitch p , and vertical gap d , for design optimization. The MoM-Line model for EFAs is validated by data from previous studies and our on-site experiments. Through analyzing the relationship between thrust force and different electrode parameters, we acquire a more reasonable design scheme and optimization direction of the EFA for different application conditions and write an open-sourced program for the general use of parameter selection.

The structure of this article is as follows. The next section introduces the modeling methods of EFAs using MoM and the revision of MoM using line charges, analysis and optimization of parameters based on the model, and materials and fabrication of electrode films. The Results section describes the verification of the models and application of the model to

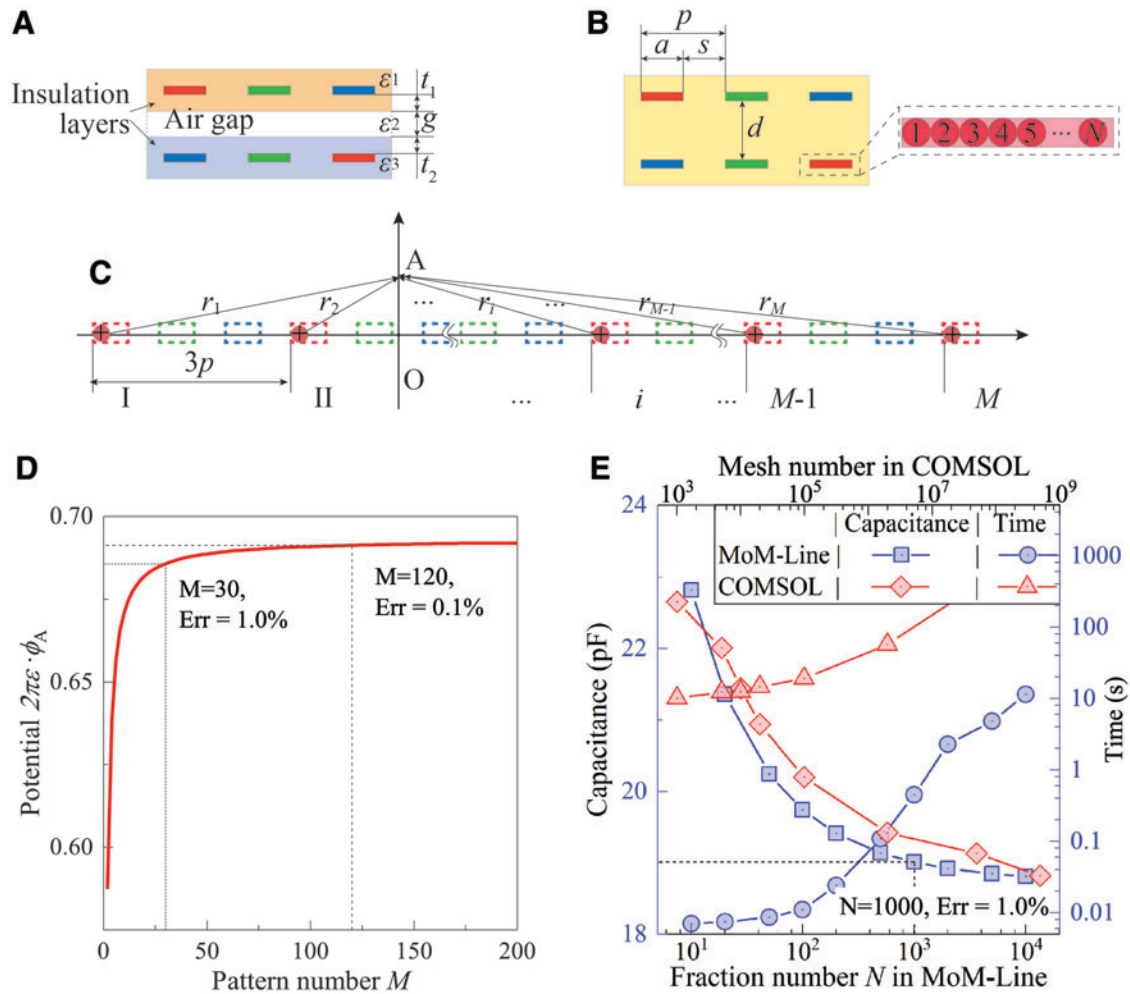


FIG. 2. Modeling of EFAs by MoM-Line. **(A)** The electrode pattern of an EFA. **(B)** The equivalent model of the electrode pattern (homogeneous dielectric material) with the lines of charge in electrodes. **(C)** A group of identical line charges. **(D)** The potential at point A [shown in **(B)**] generated by a group of identical line charges for different values of M . **(E)** Comparison of MoM-Line and FEM by computing the capacitance of a pair of parallel electrodes. FEM, finite element method; MoM, method of moments. Color images are available online.

an open-source program for parameter optimization. The last section summarizes the results and discusses future work.

Materials and Methods

Modeling

EFAs have diverse patterns, and inside most of them, multiphase electrodes are uniformly distributed on the same plane in the slider or stator film, as presented in Figure 1C. The three-phase electrode pattern is simple and easy to devise and thus became popular in previous studies on EFAs.^{11,27} This article takes the three-phase electrode pattern as an instance in the analyses, and other patterns can be investigated in a similar way.

Modeling of line charges based on MoM. The array pattern of three-phase electrodes is demonstrated in Figure 2A, where structural parameters and permittivities of different layers are marked. To simplify the multilayer structure, we transform it into an equivalent model with a homogeneous dielectric material shown in Figure 2B. The

equivalent distance between the electrodes in the two films can be calculated by

$$d = \frac{(t_1 + t_2 + g)^2 \varepsilon_1}{(t_1 + t_2) \varepsilon_1 + g \varepsilon_2}, \quad (1)$$

where t_1 and t_2 are the thicknesses of slider and stator films with relative permittivity ε_1 and g is the air gap with relative permittivity ε_2 .

We assume that each electrode comprises a large number of side-by-side line charges with infinite length, as shown in Figure 2B, since the electrode length–width ratio is sufficiently large (around 1000–10,000) in practice. The line charges are referred to as 1, 2, 3, ... N in each electrode.

The line charges at the same position of the electrodes belonging to the same phase have the same charge density and electrical potential. They are a group of identical line charges, as shown in Figure 2C (red points). If we have M units of three-phase electrodes, the superpositioned potential generated by these identical line charges can be expressed as

$$\phi = \frac{\lambda}{2\pi\epsilon} \sum_{i=1}^M \ln \frac{r_0}{r_i}, \quad (2)$$

where ϕ is the electrical potential difference between point A and point O (point O is the midpoint of electrodes in the lower film), λ is the line charge density of each line, r_0 is the radius of each charged line, r_i is the distance of point A to the i -th line of charge, and ϵ is the permittivity.

From this equation, it is evident that a higher M value can generate a higher potential at the point. In practice, M can be greater than hundred.⁹ However, in the model, a high M value costs more computational resources and hence we need to consider the trade-off while choosing the value for M in the model. In this study, to optimize the value of M , we calculated the potential at point A for a different M value. As shown in Figure 2D, the potential ϕ_A sharply increases when M is small and then gently rises when M is more than a hundred. For example, when M is 2, the error could be more than 15%. Comparatively, the error is nearly 1% if M is 30 and <0.1% if M is larger than 120. Hence, in this work, M is set to 30 in calculations for high efficiency, but low precision, and 120 in other estimations for high precision, but low efficiency.

Modeling of the electrostatic field of an EFA. Using the MoM based on line charge (MoM-Line) mentioned in the last part, we can obtain the relationship between the potential vector $U_{6N \times 1}$ and line charge vector $\Lambda_{6N \times 1}$ as follows:

$$U_{6N \times 1} = D_{6N \times 6N} \Lambda_{6N \times 1}, \quad (3)$$

where $D_{6N \times 6N}$ is the coefficient matrix calculated from Equation (2). The input voltage on the three-phase electrodes ($u_{6 \times 1} = [\sin\theta, \sin(\theta - 2\pi/3), \sin(\theta + 2\pi/3), \sin(\theta + 2\pi/3), \sin(\theta - 2\pi/3), \sin\theta]$) can also be expressed by a potential vector:

$$U_{6N \times 1} = A_{6N \times 6} u_{6 \times 1}, \quad (4)$$

where $A_{6N \times 6}$ is the transform matrix and its components are

$$a_{ij} = \begin{cases} 1 & (j-1)N < i < jN \\ 0 & \text{others} \end{cases}. \quad (5)$$

When the slider film is exactly against the stator film (the electrodes in the two films are overlapped), the coefficient matrix $D_{6N \times 6N}$ can be achieved by

$$D_{6N \times 6N} = \frac{1}{2\pi\epsilon} \sum_{i=1}^M (\ln r_0 - \ln R_{6N \times 6N}), \quad (6)$$

where $R_{6N \times 6N}$ is the relative distance matrix of different lines of charge, which can be represented by

$$R_{6N \times 6N} = \sqrt{(X^T - X)^2 + (Y^T - Y)^2}, \quad (7)$$

where X and Y are the x -position and y -position matrixes of every line, which are expressed as

$$X_{6N \times 6N} = B_1 \frac{a}{N} + B_2 p, \quad (8)$$

$$Y_{6N \times 6N} = Cd, \quad (9)$$

where the matrixes B_1 , B_2 , and C are dimensional coefficients, which can be found in Supplementary Data with more details. Thus, we can obtain the relationship between actuator structural parameters (a , s , p , and d) and the coefficient matrix $D_{6N \times 6N}$.

When relative movement occurs between the two electrode films, that is, the slider film moves by a distance of x with respect to the stator film, we only need to adjust the X -position matrix in Equation (8) by

$$X_{6N \times 6N} = B_1 \frac{a}{N} + B_2 p + x. \quad (10)$$

We can also calculate the capacitance matrix $C_{6 \times 6}$ of an EFA directly based on the MoM-Line model, which can be used to verify our model with previous studies,

$$C_{6 \times 6} = A_{6 \times 6N}^T D_{6N \times 6N} A_{6N \times 6}. \quad (11)$$

Compared with FEM simulation (usually used in calculations in previous work),²³ the algorithm based on MoM-Line can significantly reduce computation duration. Here, to contrast the two methods, we take a parallel-plate capacitor, which is also the simplest effective unit in an EFA, as an instance. The MoM-Line algorithm proposed in this work achieves very high accuracy and efficiency (relative error: 1.0%, computation duration: 0.4 s) with fraction number $N=1000$, while FEM simulation (COMSOLTM 5.5) requires an ultrafine mesh with about one million elements to obtain the same accuracy, costing 600 times longer duration (more than 4 min), as shown in Figure 2E.

Force model of EFAs. The line charge density vector $\Lambda_{6N \times 1}$, obtained using Equation (3), can be divided into $^{sl}\Lambda_{6N \times 1}$ and $^{st}\Lambda_{6N \times 1}$, which are the line charge density vectors in the slider film and the stator film, respectively. The relative position matrix $R_{6N \times 6N}$ can also be divided into a slider-stator relative position matrix $^{ll}R_{3N \times 3N}$, slider-slider relative position matrix $^{ll}R_{3N \times 3N}$, and stator-stator relative position matrix $^{st}R_{3N \times 3N}$:

$$R_{6N \times 6N} = \begin{bmatrix} ^{ll}R_{3N \times 3N} & ^{ll}R_{3N \times 3N} \\ ^{ll}R_{3N \times 3N} & ^{st}R_{3N \times 3N} \end{bmatrix}, \quad (12)$$

among which $^{ll}R_{3N \times 3N}$ equals $^{st}R_{3N \times 3N}$.

Therefore, the output force \mathbf{F} of an EFA can be obtained based on Coulomb's law,

$$\mathbf{F} = \frac{1}{2\pi\epsilon} g_{1 \times 3N}^T \frac{^{sl}\Lambda_{6N \times 1} \otimes ^{st}\Lambda_{6N \times 1}}{^{ll}R_{3N \times 3N} * ^{ll}R_{3N \times 3N}} g_{3N \times 1} = F_{th} \mathbf{e}_x + F_{ad} \mathbf{e}_y, \quad (13)$$

where F_{th} is the ideal thrust force, F_{ad} is the adhesive force between two films, $g_{3N \times 1}$ is a transformation vector, \otimes is the

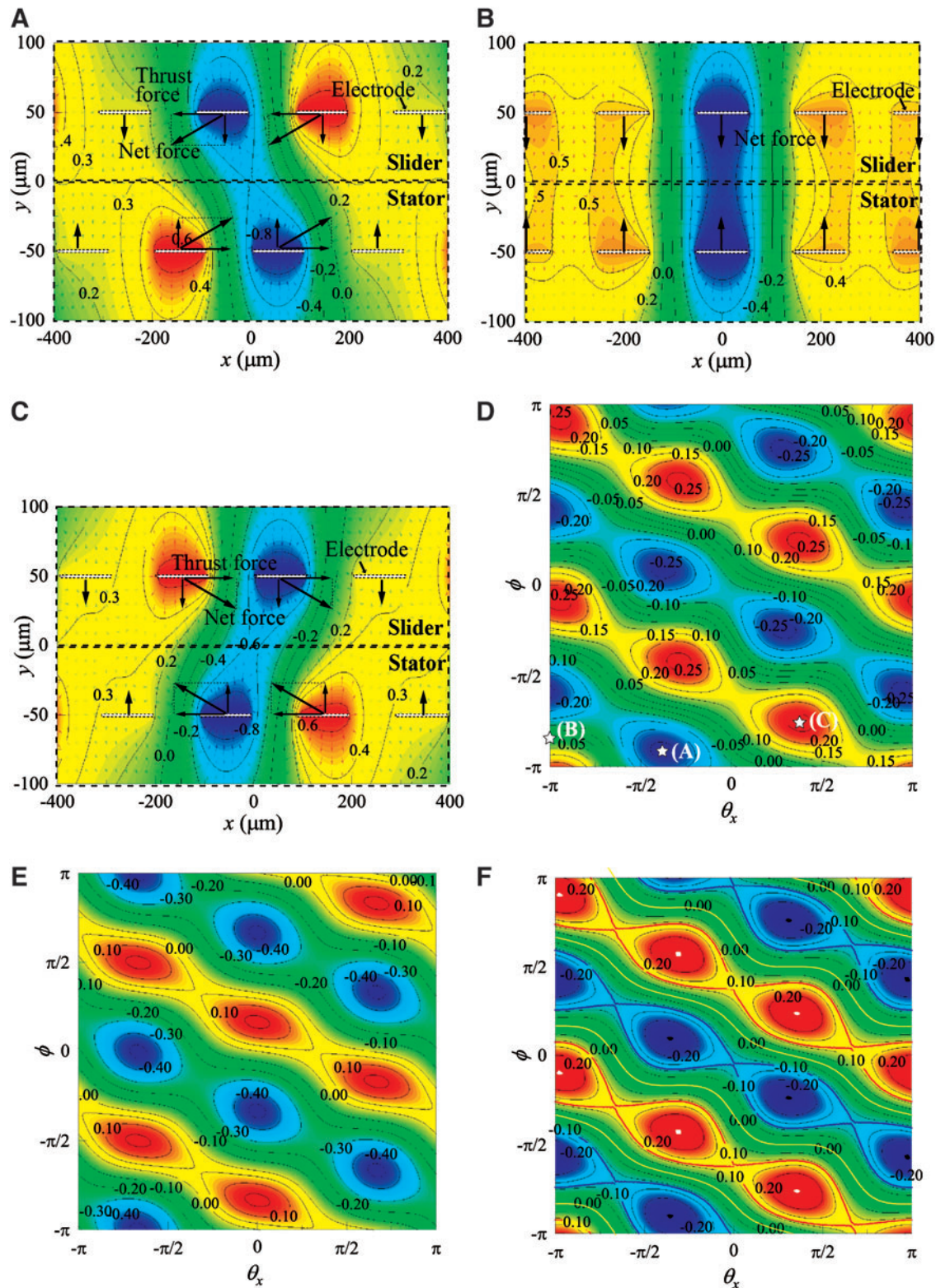


FIG. 3. Electric distribution and fluctuation in forces calculated by MoM-Line when an EFA is moving. (A) Electric potential and strength distribution when the actuator produces the maximum ideal thrust force ($\theta_x = -0.38\pi$ and $\phi = 0.08\pi$). (B) Electric potential and strength distribution when the actuator produces zero ideal thrust force ($\theta_x = 0$ and $\phi = 0.16\pi$). (C) Electric potential and strength distribution when the actuator produces a minimum ideal thrust force ($\theta_x = 0.38\pi$ and $\phi = 0.24\pi$). (D) The contour of ideal thrust force, including the corresponding forces (marked by stars) for cases shown (D.A–D.C). (E) Contour of adhesive force. (F) The contour of actual thrust force, where white dots are the maximum pulling force, black dots are the maximum pushing force, yellow curves are zero force, red curves are the maximum stable pulling force, and blue curves are the maximum stable pushing force. Color images are available online.

operator of the Kronecker product, and $*$ is the operator of the Hadamard product.

The actual thrust force is affected by the friction force. The friction force is complicated and influenced by materials, surface cleanness, and lubrication methods, but mainly exerted by the adhesive force F_{ad} . Therefore, the actual thrust force \hat{F}_{th} can be achieved by

$$\hat{F}_{th} = F_{th} - \mu F_{ad}, \quad (14)$$

where μ is the coefficient of friction.

Instead of calculating the output force using Coulomb's law directly, previous studies use the capacitance matrix $C_{6 \times 6}$ to acquire the thrust force.^{20–22} In this way, it is required to simulate out every component of the capacitance matrix at a different location x at first and then fit these components using separate fitting formulas.

The capacitance matrix $C_{6 \times 6}$ has good symmetry, as displayed by

$$C_{6 \times 6} = \begin{bmatrix} c_s & c_f & c_f & c_{g_1} & c_{g_2} & c_{g_3} \\ c_f & c_s & c_f & c_{g_3} & c_{g_1} & c_{g_2} \\ c_f & c_f & c_s & c_{g_2} & c_{g_3} & c_{g_1} \\ c_{g_1} & c_{g_3} & c_{g_2} & c_s & c_f & c_f \\ c_{g_2} & c_{g_1} & c_{g_3} & c_f & c_s & c_f \\ c_{g_3} & c_{g_2} & c_{g_1} & c_f & c_f & c_s \end{bmatrix}, \quad (15)$$

where the components c_s , c_f , c_{g_1} , c_{g_2} , and c_{g_3} are functions of the position in electric angle θ_x ($\theta_x = 2\pi x/3p$). Then, the ideal thrust force can be obtained:

$$F_{th} = \frac{1}{2} u_{1 \times 6}^T \frac{dC_{6 \times 6}}{dx} u_{6 \times 1}. \quad (16)$$

In this method, we only obtain the ideal thrust force and cannot calculate the adhesive force while the actuator is running. Besides, this process is laborious and error-prone.

Figure 3A–C shows the electric potential and electric strength distribution around the electrodes of an EFA using

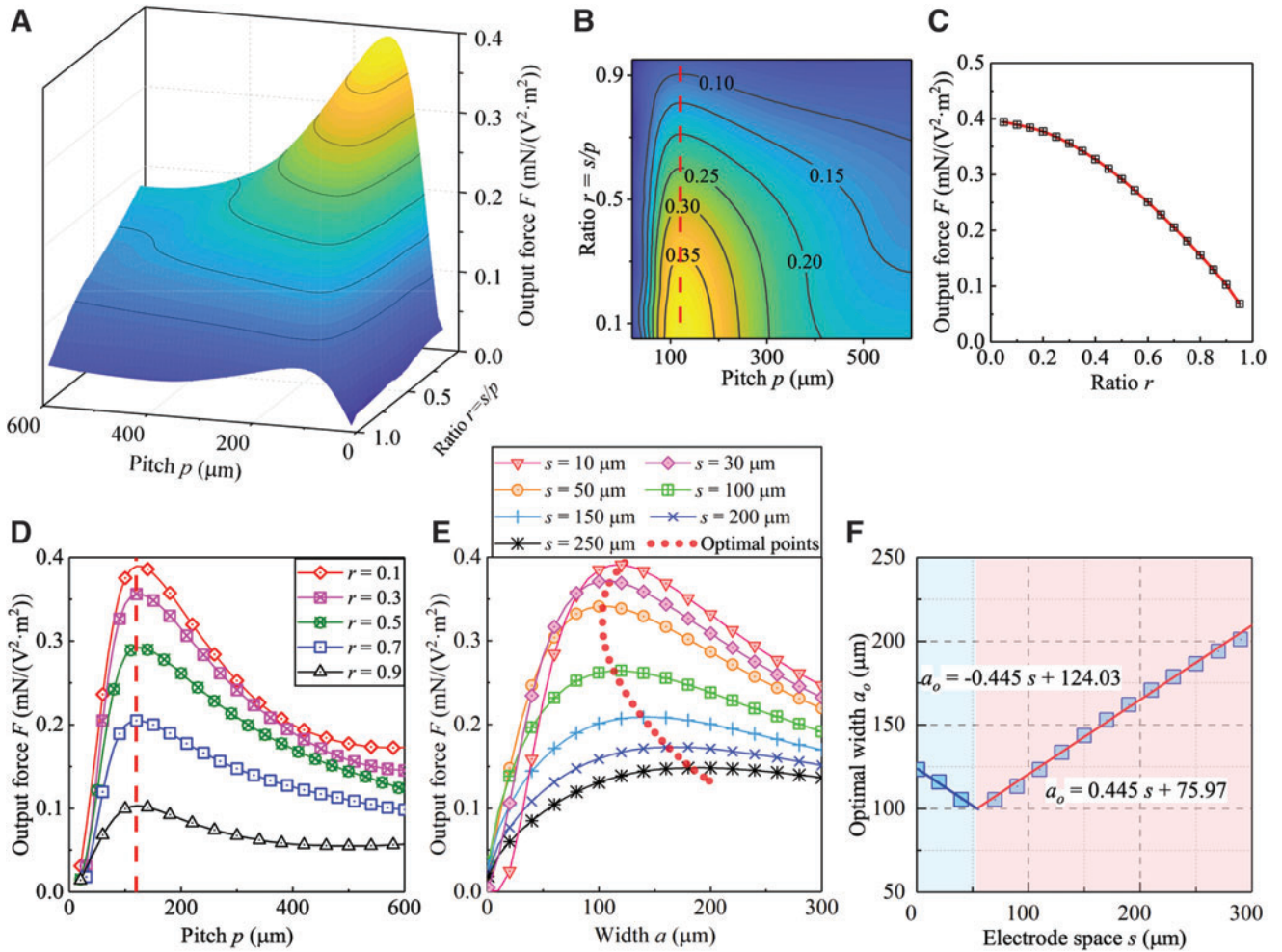


FIG. 4. Influence of width, space, and pitch. (A) The output force of the surface when the vertical gap d is 100 μm. (B) The output force contour of the surface, while the red dashed line shows the ridge where the force always reaches its peak value. (C) The relationship plot between output force and the ratio at the optimal pitch p_o (120 μm). (D) The plots between output force and electrode pitch at different ratios, and the red dashed line indicates peak values. (E) Plots between output force and electrode width at various fixed spaces, where the red dotted line fits the optimal points of each curve. (F) The relationship between the optimal width and electrode space. Color images are available online.

the MoM-Line algorithm. We could adjust the voltage phase φ and position in the electric phase θ_x to achieve the maximum, zero, and minimum ideal thrust force of the EFA. Owing to the periodicity of the position in the electric phase θ_x and the supplied voltage phase φ , the ideal thrust force and adhesive force of the actuator fluctuate periodically, demonstrated in Figures 3D and 2E. Taking friction into consideration (e.g., $\mu=0.1$), the maximum and minimum points in the actual thrust force contour shift a little, which depends on the friction coefficient. According to Figure 3F, the maximum points (white points) and minimum points (black points) indicate the maximum load that the actuator can sustain in pull and push. When operating loads are larger than \hat{F}_{th0} (red curves) or lesser than \hat{F}_{th1} (blue curves), the actuator cannot maintain continuous running. In other words, it will vibrate in its position. When the operating load is between \hat{F}_{th0} (red curves) and \hat{F}_{th1} (blue curves), the actuator can move continuously.

Parameter analysis and optimization

Using the model (MoM-Line) described in the last section, here we evaluate different parameters, including electrode width a , electrode space s , electrode pitch p , and gap d , as shown in Figure 2B, to optimize the output force.

Influence of the electrode width, space, and pitch. In the horizontal direction, three primary interplaying parameters (i.e., a , s , and p) are critical for the output force, and they have such a relationship: $a + s = p$. Among them, the pitch is often selected as a reference to compare the force of different patterns since it represents the electrode density and also

determines the velocity of the actuator directly.²¹ On another aspect, the space s can be the first concern if we compare the forces considering the same maximum electrical breakdown field between electrodes or the limitations of the fabrication. Therefore, we take these concerns into consideration for parameter selection in the following discussion.

Based on the models in the Materials and Methods section, we compute the thrust force under a unit voltage, with a variable pitch p and space ratio r ($r = s/p$) at a constant vertical gap d (100 μm), and the results are shown in Figure 4A. It is noted that the thrust force for each set of dimensional parameters is the maximum value found in Figure 3F (white dots). From these data in Figure 4A, we can optimize the parameters considering different limitations.

If the pitch is the first concern in parameter optimization, we can analyze them as follows. For different pitches, there is an optimal value where the output force per volt achieves the maximum, as shown in Figure 4B (ridgeline marked by the red dashed line). The output force goes down quickly when the pitch is less than the optimal point, whereas the output force declines gently at a pitch larger than the optimal value. This phenomenon is perhaps because electrodes that are too close cause electrical field interference and electrodes that are too far generate a less attractive force. Interestingly, the optimal pitches at different space/pitch ratios remain the same at 120 μm , as plotted in Figure 4D. Therefore, based on this knowledge, we can directly determine the optimal pitch, which is irrelevant to the space ratio. On the other hand, with the increasing space ratio when the pitch is the same, the output force per volt becomes lower, as shown in Figure 4C. This phenomenon means the electrode space should be as small as possible because closer electrodes result in a higher

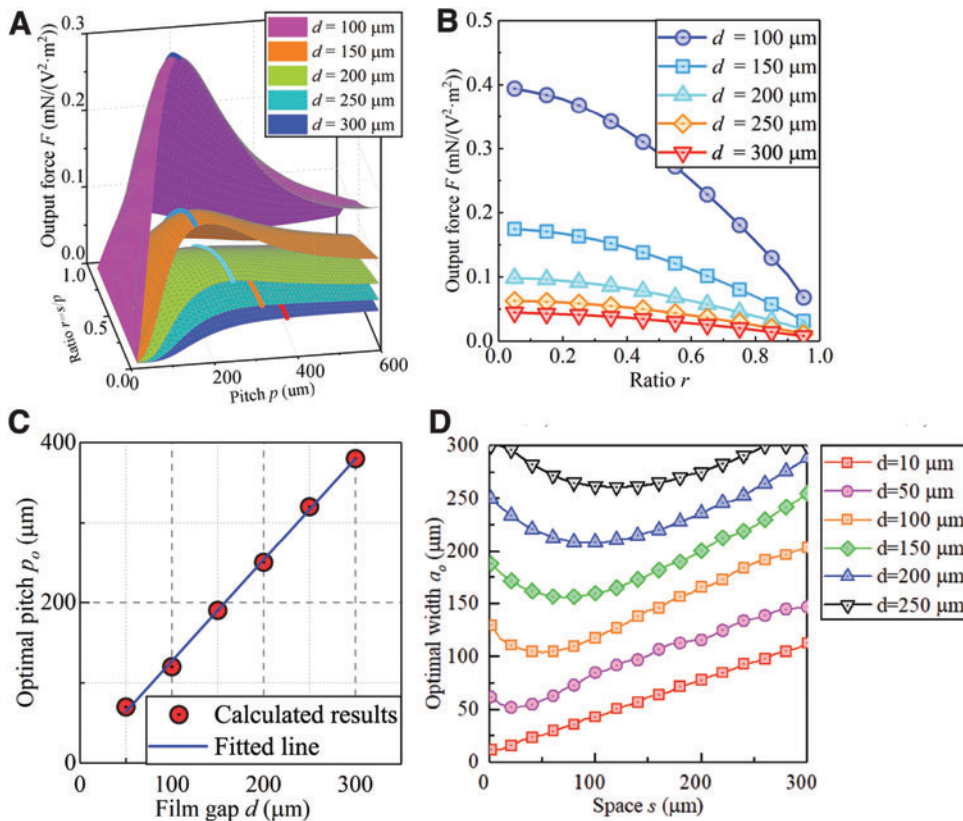


FIG. 5. Influence of the vertical gap. (A) Output forces for various film gaps, where the colored lines are the peak ridges of each surface. (B) The optimal output force for different space ratios and the corresponding optimal pitches and vertical gaps. (C) The optimal pitches for different film gaps. (D) The optimal width determined by the space at different vertical gaps. Color images are available online.

electric field in the electrode films. In practice, the space and ratio are usually limited by manufacturing conditions.

On another side, if the space s is the main limitation, we can optimize the parameters as follows. When we keep the space constant, the optimal value of electrode widths can be found in Figure 4E. If the space s changes, the optimal width a_o varies almost linearly in two segments, as shown in Figure 4F:

$$a_o = \begin{cases} -0.445s + 124.03 & s < 54 \\ 0.445s + 75.97 & s \geq 54 \end{cases} \quad (17)$$

Based on these equations, we can select a suitable width for the given space.

Influence of the vertical gap between electrodes. The vertical gap d has a great impact on the output force of the actuator too. Based on MoM-Line, we calculate the output

forces with p and r at different film gaps and illustrate them in Figure 5A. For the optimal value of pitch and gap, the maximum forces are at the ridgelines shown in Figure 5A. These curves are also extracted and plotted in Figure 5B. Comparing these curves, it is obvious that the maximum output force becomes larger while the gap decreases since closer electrodes generate a higher, electrostatic attractive force. Similar to Figure 4C, the output force decreases with the increasing ratio since the areas of electrodes and the effective capacitance decline.

In the last part, from data in Figure 4B and D, we find that the optimal pitch p_o remains the same for different values of r . This rule also takes effect at different values of d , but the optimal pitch value changes with the gap. We plot the optimal pitch with variable film gap, as shown in Figure 5C, and fit it in a line:

$$p_o = 1.263d + 0.667. \quad (18)$$

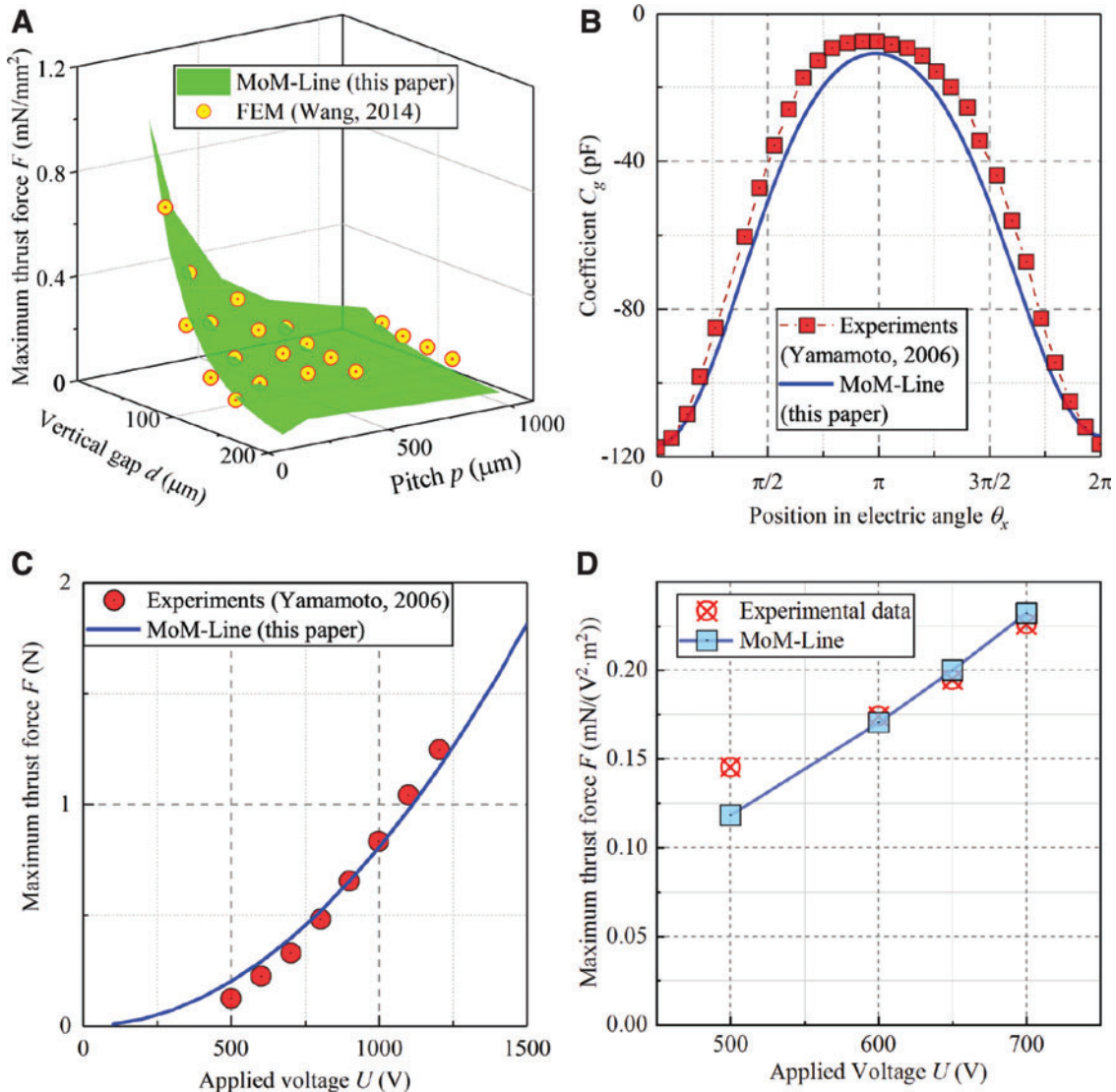
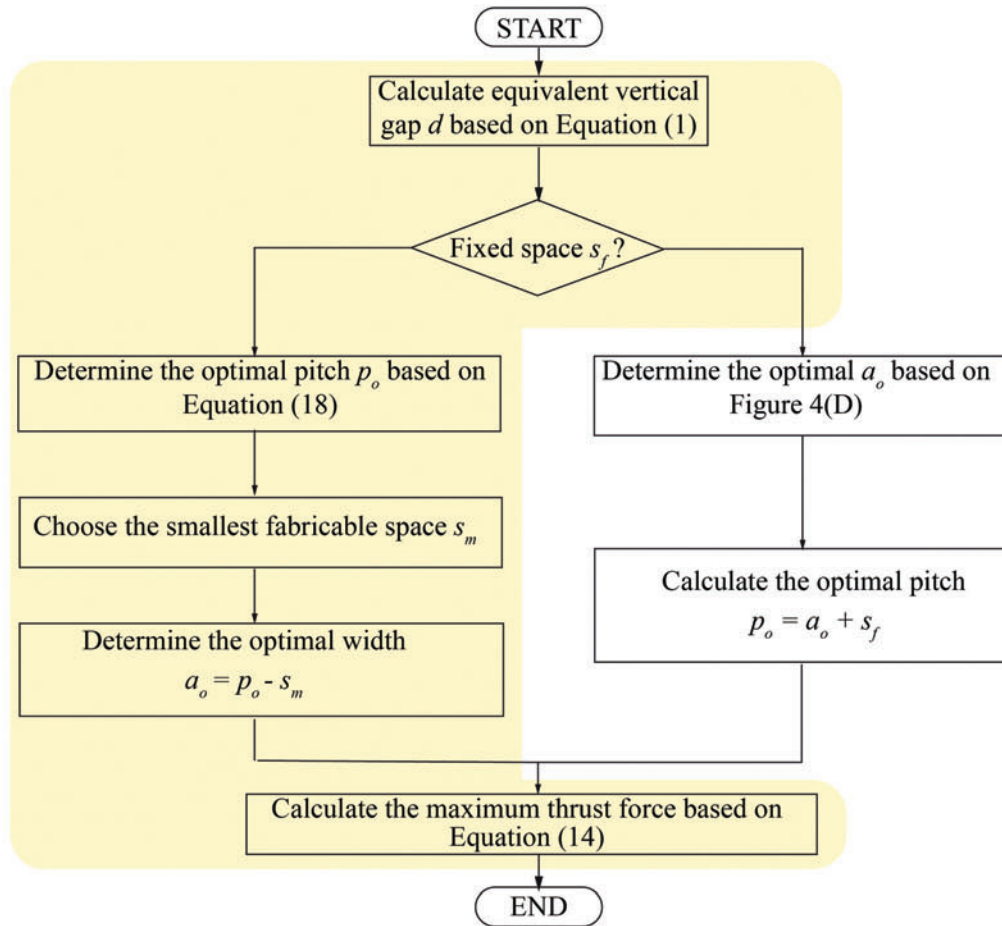


FIG. 6. Validation with simulation and experiments. (A) Comparison of thrust force calculated by MoM-Line and FEM in previous work. (B) Comparison of capacitance coefficients estimated by MoM-Line in this work and those achieved from experiments in previous work. (C) Comparison of maximum thrust force estimated by MoM-Line in this work and that achieved from experiments in previous work. (D) Comparison of maximum thrust force estimated by MoM-Line and that obtained from experiments in our laboratory. Color images are available online.

A



B

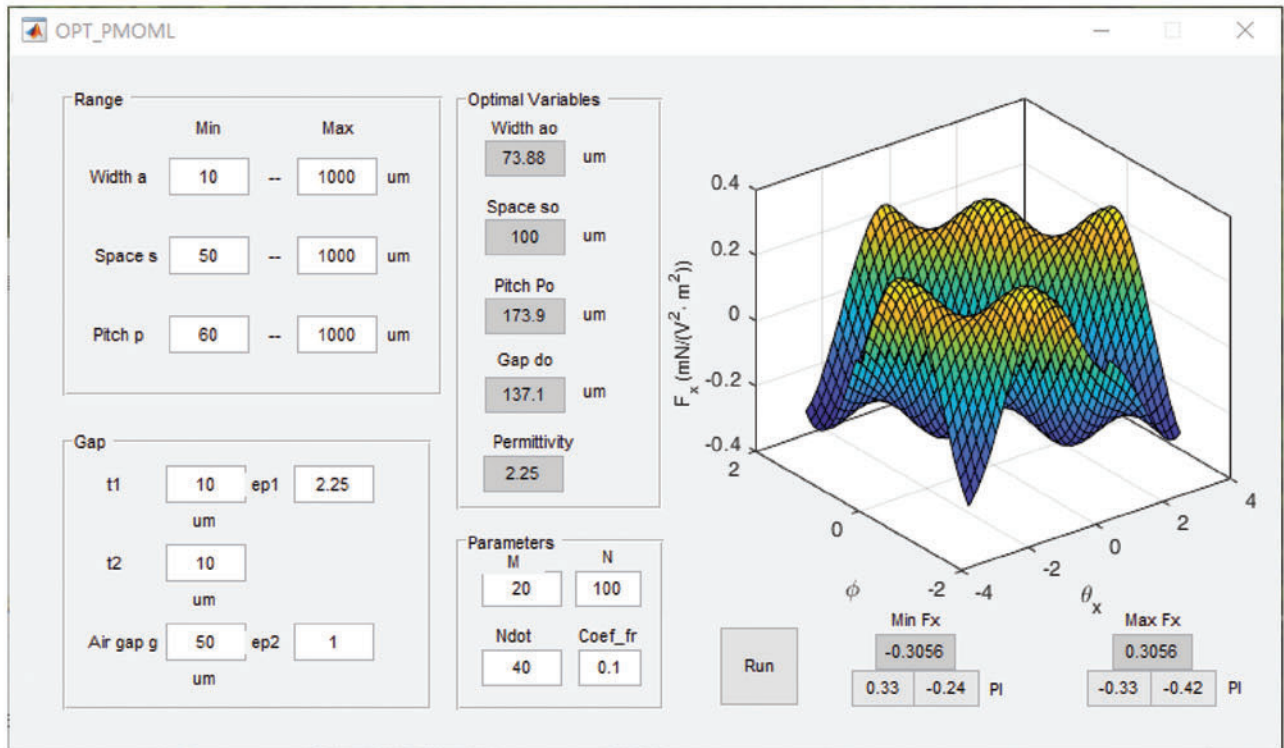


FIG. 7. The optimization workflow and an example program. (A) Flow diagram for EFA parameter optimization based on MoM-Line, where the yellow section has been implemented by a MATLAB program. (B) A sample application executed by a MATLAB GUI capable of estimating optimal structural parameters for the maximum thrust force under unit voltage. Color images are available online.

Therefore, to design an EFA with the most significant output force, we need first to find the smallest film gap, then calculate the optimal pitch using Equation (18), and last, make the ratio as low as can be fabricated. On the other hand, the optimal value of width varies with the space, as shown in Figure 5D. When the space s is determined in advance, the optimal width a_o should be chosen in this figure.

Materials and fabrication of electrode films

To verify the model, we fabricated several pieces of electrode films, as shown in Figure 1A. In each electrode film, there is a layer of three-phase electrodes patterned on the substrate layer made from polyimide. The electrode width and space are both $100\ \mu\text{m}$. The electrodes were made of copper with a thickness of $12\ \mu\text{m}$ by photolithography and chemical etching. Electrodes of the same phase are connected by bus lines through holes. Above the electrodes, the cover layer was made of a polyimide layer and an acrylic adhesive layer. These layers were bonded together by heat press for insulation of conductors.

Results

Validation

In this study, we compare the proposed model with previous methods and verify it by experimental results from both previous literature and the current work.

Figure 6A shows the actuation force calculated from our model compared with those from FEM in previous research,^{21,23} and the maximum difference is only 5%. Considering the smaller computation consumption, this model is more suitable for fast calculation without losing accuracy, or a higher accuracy calculation within the same duration.

Besides, this model can also estimate the characteristic capacitance matrix with high accuracy, which is one of the most critical parameters to evaluate actuators. Figure 6B compares the gap capacitance coefficient c_g calculated by our model and experimental results in a previous article²¹ ($a = 100\ \mu\text{m}$, $s = 100\ \mu\text{m}$, and $d = 64\ \mu\text{m}$), and the maximum error is only 10%. Because of the good coincidence with capacitance coefficients, the modeled thrust force matches the corresponding experimental results very well (12% error at maximum), too, as shown in Figure 6C. We also validated the MoM-Line with an existing EFA in our laboratory ($a = 100\ \mu\text{m}$, $s = 100\ \mu\text{m}$, film thickness $t_1 = t_2 = 64\ \mu\text{m}$, and estimated air gap $g = 124\ \mu\text{m}$). The actuator is shown in Figure 1A, and results are shown in Figure 6D. Its equivalent vertical gap d was $345.95\ \mu\text{m}$ based on Equation (1). The maximum thrust forces experimented and calculated are in good accordance (5% error at maximum, except data at 500 V). Therefore, the MoM-Line model presented here has been proven to be feasible and effective. Note that the great difference at 500 V is perhaps caused by the larger air gap between electrode films (resulting in smaller normal adhesive force and friction force) and fewer induced charges on the electrode film surface (negatively influencing the thrust force) rising by the weaker electrical field. These factors are not considered in our current models, but can be explored further in the future.

Application

Based on our model, we design a flow diagram to help researchers determine the optimal structural parameters of EFAs under different circumstances. In the flow diagram shown in

Figure 7A, we decouple the complicated relationships between parameters and make it possible to optimize them in a linear way. Accordingly, we write an optimization program to find the optimal structural parameters of an EFA and make it open-sourced online.²⁸ Its GUI is shown in Figure 7B, and users can use it to select parameters and optimize their EFAs. Through the GUI, users input the ranges of structural parameters and several material coefficients, and the program can calculate optimal parameters and distribution of thrust force.

As an example, we optimized an EFA in our laboratory. The input numbers for structural parameters and material coefficients are shown in Figure 7B, and the program outputs the optimal parameters ($a = 73.88\ \mu\text{m}$, $s = 100\ \mu\text{m}$, $p = 173.88\ \mu\text{m}$, and $d = 137.1\ \mu\text{m}$) and the corresponding thrust force [$0.3056\ \text{mN}/(\text{V}^2 \cdot \text{m}^2)$], 23.6% greater than existing actuators with the same space between electrodes ($a = 100\ \mu\text{m}$, $s = 100\ \mu\text{m}$, $p = 200\ \mu\text{m}$, and $d = 137.1\ \mu\text{m}$). If we further broaden the parameter range based on a more advanced fabrication technique, the maximum force can be even higher. When the lower limit of space and air gap reaches $10\ \mu\text{m}$, the maximum thrust force achieved is nearly $6\ \text{mN}/(\text{V}^2 \cdot \text{m}^2)$ with the optimal parameter set ($a_o = 37.17\ \mu\text{m}$, $s = 10\ \mu\text{m}$, $p_o = 47.17\ \mu\text{m}$, and $d = 36.82\ \mu\text{m}$).

Conclusions

In this article, we have built a numerical model showing the relationship between structural parameters, material parameters, and output force for EFAs. The model is based on the MoM using uniformly distributed line charges as basic elements in EFAs. In contrast with the previous multistep methods, that is, first obtaining the capacitance matrix by simulation or experiments and then fitting and taking the derivative of the capacitance matrix to calculate the output force of an EFA, the MoM-Line builds a direct relationship between parameters and output force of EFAs. In the meantime, the method can, except for deducing the distribution of electric potential and field strength during actuator movement, calculate the fluctuation in thrust force in the lateral direction and adhesive force in the normal direction. It enables understanding and evaluating the resultant actuation force more comprehensively. In comparison, the results calculated by MoM-Line are in excellent accordance with the previous studies. We also validate the model with existing EFAs in our laboratory to prove the validity and feasibility of the model. In total, the MoM-Line supposed in this article uses shorter computing time and fewer computing resources, but obtains more detailed information about the actuators.

We have calculated a large number of results of EFAs with different structural parameters to comprehend the output force of EFAs. Based on the parameter analysis, we summarize several rules about parameter optimization of EFAs and build an overall optimization flow diagram to facilitate designs for different operation circumstances (e.g., considering the space or pitch at first). Consequently, we write an open-sourced program for parameter selection and optimization as an example. In summary, this work provides a novel method to build a comprehensive model of EFAs, which is expected to benefit both fundamental studies and applications of EFAs.

In the future, this method can be further modified to analyze EFAs with more complex electrode shapes, composite materials, and electrode films.

Acknowledgments

The authors acknowledge the assistance of SUSTech Core Research Facilities.

Author Disclosure Statement

No competing financial interests exist.

Funding Information

This work is supported by the National Natural Science Foundation for Young Scientists of China (51905256), the Natural Science Foundation of Guangdong Province of China (2020A1515010955), and the Key Technology Innovation Special Funds for Key Industries of the Chongqing Science and Technology Bureau (cstc2019jcsx-fxydX0017).

Supplementary Material

Supplementary Data

References

- Guo J, Bamber T, Chamberlain M, *et al.* Optimization and experimental verification of coplanar interdigital electroadhesives. *J Phys D Appl Phys* 2016;49:1–18.
- Majidi C. Soft robotics: A perspective—Current trends and prospects for the future. *Soft Robot* 2014;1:5–11.
- Schaler EW, Ruffatto D, Glick P, *et al.* An electrostatic gripper for flexible objects. In 2017 IEEE/RSJ International Conference on Intelligent Robots and Systems (IROS). Vancouver, Canada: IEEE, September 24, 2017, pp. 1172–1179.
- Schaler EW, Zohdi TI, Fearing RS. Thin-film repulsive-force electrostatic actuators. *Sensor Actuat A Phys* 2018; 270:252–261.
- Guo J, Leng J, Rossiter J. Electroadhesion technologies for robotics: A comprehensive review. *IEEE Trans Robot* 2019; 36:313–327.
- Shintake J, Rosset S, Schubert B, *et al.* Versatile soft grippers with intrinsic electroadhesion based on multifunctional polymer actuators. *Adv Mater* 2016;28:231–238.
- Rogers JA, Someya T, Huang Y. Materials and mechanics for stretchable electronics. *Science* 2010;327:1603–1607.
- Higuchi T. Next generation actuators leading breakthroughs. *J Mech Sci Technol* 2010;24:13–18.
- Wang H, Yamamoto A, Higuchi T. A crawler climbing robot integrating electroadhesion and electrostatic actuation. *Int J Adv Robot Syst* 2014;11:1–11.
- Hosobata T, Yamamoto A, Higuchi T. Modeling and analysis of a linear resonant electrostatic induction motor considering capacitance imbalance. *IEEE Trans Indus Electron* 2014;61:3439–3447.
- Hosobata T, Yamamoto A, Higuchi T. Transparent synchronous electrostatic actuator for long-stroke planar motion. *IEEE ASME Trans Mechatron* 2015;20:1765–1776.
- Zhang Z, Yamashita N, Yamamoto A, *et al.* Modeling and system identification of three-layer structure electrostatic film motors for a robotic fish. In Proceedings of the 2009 IEEE International Conference on Mechatronics and Automation, IEEE, Changchun, 2009, pp. 2729–2734.
- Akio Y, Toshiaki N, Takahisa B, *et al.* A high-power electrostatic motor using skewed electrodes. *Electr Eng Japan* 1998;125:50–58.
- Laschi C, Mazzolai B, Cianchetti M. Soft robotics: Technologies and systems pushing the boundaries of robot abilities. *Sci Robot* 2016;1:1–11.
- Gu G-Y, Zhu J, Zhu L-M, *et al.* A survey on dielectric elastomer actuators for soft robots. *Bioinspir Biomim* 2017;12:011003.
- Liu K-C, Friend J, Yeo L. A brief review of actuation at the micro-scale using electrostatics, electromagnetics and piezoelectric ultrasonics. *Acoust Sci Technol* 2010;31:115–123.
- Bahramzadeh Y, Shahinpoor M. A review of ionic polymeric soft actuators and sensors. *Soft Robot* 2014;1:38–52.
- Zhang Z, Yamashita N, Gondo M, *et al.* Electrostatically actuated robotic fish: Design and control for high-mobility open-loop swimming. *IEEE Trans Robot* 2008;24:118–129.
- Wang H, Yamamoto A. A thin electroadhesive inchworm climbing robot driven by an electrostatic film actuator for inspection in a narrow gap. In IEEE International Symposium on Safety, Security, and Rescue Robotics (SSRR), Linköping, 2013, pp. 1–6.
- Wang H, Yamamoto A, Toshiro H. Electrostatic motor driven electroadhesive robot. In IEEE/RSJ International Conference on Intelligent Robots and Systems. Vilamoura, Portugal: IEEE, 2012, pp. 914–919.
- Yamamoto A, Niino T, Higuchi T. Modeling and identification of an electrostatic motor. *Precis Eng* 2006;30:104–113.
- Zhang G, Yamamoto A. Toward self-sensing of an electrostatic film motor using driving currents. In IEEE International Conference on Industrial Technology (ICIT), Lyon, 2018, pp. 551–556.
- Wang H, Yamamoto A, Toshiro H. The effect of parameters on the output forces of the integration of electroadhesion and electrostatic actuation considering breakdown voltage. In The Japan Society for Precision Engineering Spring Conference, Kanazawa, Japan, 2014, pp. 259–260.
- Zhang G, Yamamoto A. Comparative analysis for sensorless displacement estimation of electrostatic film motors in different motor configurations. In IEEE International Conference on Industrial Technology (ICIT). Melbourne: IEEE, 2019, pp. 163–168.
- Wang W, Wang Q, Ren H, *et al.* Electrostatic repulsive out-of-plane actuator using conductive substrate. *Sci Rep* 2016; 6:35118–35128.
- He J, Xie J, He X, *et al.* Calculating capacitance and analyzing nonlinearity of micro-accelerometers by Schwarz–Christoffel mapping. *Microsyst Technol* 2014;20:1195–1203.
- Wang H, Yamamoto A. Analyses and solutions for the buckling of thin and flexible electrostatic inchworm climbing robots. *IEEE Trans Robot* 2017;33:889–900.
- Wang W. Implementation of MoM-Line of EFA by Matlab. 2020. https://github.com/shzhlwgg/MoM_Line-of-EFA (accessed September 24, 2020).

Address correspondence to:

Hongqiang Wang
 Department of Mechanical and Energy Engineering
 Southern University of Science and Technology
 No 1088, xueyuan Blvd., Xili
 Nanshan District, Shenzhen
 Guangdong 518055
 China

E-mail: wanghq6@sustech.edu.cn